# Analyst

## Accepted Manuscript
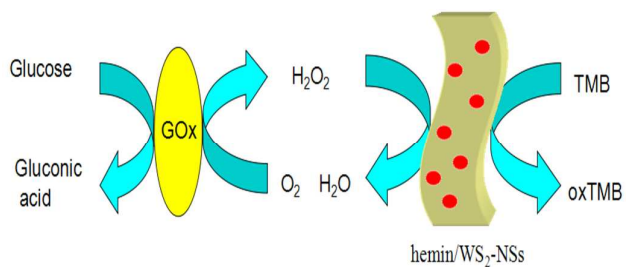
Hemin-functionalized $WS_2$ nanosheets as highly active peroxidase mimetic for label-free colorimetric detections of $H_2O_2$ and glucose was reported.

# Analyst

## PAPER

# Hemin-functionalized WS$_2$ nanosheets as highly active peroxidase mimetic for label-free colorimetric detections of H$_2$O$_2$ and glucose

Qiao Chen [ab], Jia Chen [a], Cunji Gao [a], Mingliang Zhang [a], Junying Chen [b] and Hongdeng Qiu*[a]

**Hemin-functionalized WS$_2$ nanosheets (hemin/WS$_2$-NSs) was firstly obtained by the hemin assembled on the surface of few-layered WS$_2$ nanosheets (WS$_2$-NSs) *via* van der Waals interactions. Significantly, this new material possessed the advantages of both hemin and WS$_2$ nanosheets and exhibited some unique properties. Firstly, Hemin/WS$_2$-NSs had intrinsic peroxidase-like activity, which could effectively catalyze oxidation of the substrate 3,3′,5,5′-tetramethylbenzidine (TMB) by H$_2$O$_2$ to produce a typical blue color reaction. Secondly, the activity of hemin/WS$_2$-NSs was much higher than the activity of hemin or WS$_2$-NSs alone. The catalytic activity followed the typical Michaelis–Menten kinetics and was dependent on temperature, pH, H$_2$O$_2$ concentration, as well as reaction time. Based on this finding, a new highly sensitive and selective colorimetric method for H$_2$O$_2$ and glucose detection was developed. This method was simple, inexpensive for glucose detection using glucose oxidase (GOx) and hemin/WS$_2$-NSs with a linear range from $0.5 \times 10^{-5}$ to $2.0 \times 10^{-4}$ mol L$^{-1}$ with a detection limit of $1.5 \times 10^{-6}$ mol L$^{-1}$. The good catalytic activity and low-cost make the hemin/WS$_2$-NSs a useful biocatalyst for a wide range of potential applications in environmental chemistry, biotechnology and clinical diagnostic.**

## 1. Introduction

Colorimetric methods are particularly attractive for point-of-use applications because they can be visually and simply observed by the naked eye.[1,2] Colorimetric biosensing does not require expensive or sophisticated instrumentation and can be applied to field analysis and point-of-care diagnosis.[3–6] With the advent of nanotechnology, Enzyme-mimetic nanomaterials have emerged as a new class of ideal and important tools for colorimetric detection.[7,8] Nanomaterials represent promising candidates for artificial peroxidase mimetics possess significant advantages over natural enzymes (such as horseradish peroxidase, HRP) including high stability, low-cost of preparation, simple storage, flexibility in composition and structure design, tunable catalytic activities.[9] To this end, the artificial peroxidase mimetics with good catalytic properties will possess a brilliant future in enzyme-related applications. The Fe$_3$O$_4$ magnetic nanoparticles (MNPs) was first reported that possessed intrinsic peroxidase-like activity,[10] and some other metal oxide nanomaterials were also found to possess intrinsic peroxidase-like activity, such as MoS$_2$ nanosheets,[11] ZnFe$_2$O$_4$ MNPs,[12] Co$_3$O$_4$ NPs,[13] and V$_2$O$_5$ nanowires.[14] Furthermore, carbon nanomaterials such as single-wall,[15] helical carbon nanotubes,[16] graphene oxide,[17] carbon nanodots,[18] and multicolor luminescent carbon nanoparticles[19] have also been proved to possess intrinsic peroxidase catalytic activity. So far, all these enzyme-like nanomaterials have already found wide applications in a variety of fields, including biosensing,[20,21] immunoassays,[10] cancer diagnostics and therapy, neuroprotection, stem cell growth, pollutant removal,[7] and so on.

Tungsten disulfide (WS$_2$) transitions from indirect-gap semiconductor with a gap of 1.3 eV in bulk to direct-gap in a monolayer, the indirect-to-direct gap transition results in strong enhancement of photoluminescence efficiency.[22,23] So far, WS$_2$ nanosheets have received considerable attention in hydrogen evolution reactions,[24,25] energy storage,[26] electronic devices,[27] biomedicine[28], biosensors[29,30] et al. Lin's group[31] recently reported that WS$_2$ nanosheets possessed intrinsic peroxidase-like catalytic activity. The WS$_2$ nanosheets could catalyze the oxidation of TMB by H$_2$O$_2$ to produce the typical blue color reaction. On the basis of this finding, colorimetric methods for the detection of H$_2$O$_2$ and glucose were developed. Hemin (iron protoporphyrin) is the active center of the heme-protein family including cytochromes, peroxidases, myoglobins, and hemoglobins, which has the peroxidase-like activity similar to the peroxidase enzyme.[32] It also possesses a large extinction coefficient in the visible-light region, predictable rigid structures, and prospective photochemical electron-transfer ability. However, the catalytic activity of hemin was limited because of its oxidative self-degradation and molecular aggregation to inactive dimers in aqueous solution. A way to solve this problem

is immobilizing hemin on high surface area materials. As we know that the deposition of porphyrin on the graphene oxide sheets through π-π interaction was successfully realized.[33,34] Based on the above works, we thought that it might be possible for $WS_2$ nanosheets to serve as an available platform because of its similar 2D structure with graphene, which could be used to form composite nanomaterials with some plane-like molecules. If the Hemin-functionalized $WS_2$ nanosheets (hemin/$WS_2$-NSs) could be obtained, it will provide excellent opportunities for applications in the field of artificial enzyme mimetic for biosensor and biocatalysis.

In this paper, hemin/$WS_2$-NSs were a synthesized by simple wet-chemical strategy via van der Waals interactions. Significantly, the new nanocomposite possessed both excellent properties of $WS_2$ and hemin. It was found that $WS_2$ not only could effectively loaded hemin, but also provided a beneficial microenvironment for keeping the high activity of hemin. The activity of hemin/$WS_2$-NSs was much higher than the activity of hemin alone. Based on this finding, a new label-free colorimetric sensor for $H_2O_2$ and glucose was successfully developed (Scheme 1). The developed method exhibited good sensitivity and selectivity.
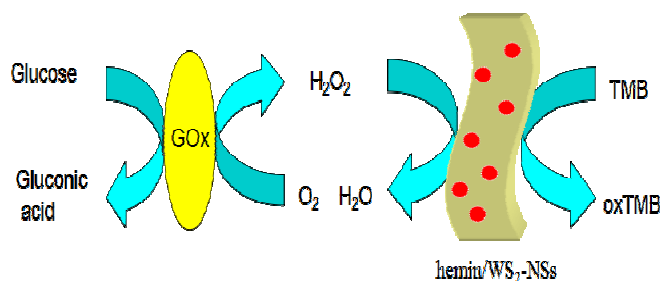


**Scheme 1**. Schematic illustration of colorimetric detection of glucose by using glucose oxidase (GOx) and hemin/$WS_2$-NSs-catalyzed reactions.

## 2. Experimental section

### 2.1. Materials and Instrumentation

Tungsten disulfide ($WS_2$) nanosheets (26 μg/mL, 1–4 monolayers, >99% Purity in dry phase) were purchased from XFNANO Materials Tech Co., Ltd (Nanjing, China). Hemin, o-phenylenediamine (OPD), 3,3′,5,5′-tetramethylbenzidine (TMB) and 2,2′-azino-bis(3-ethylbenzothiazoline-6-sulfonic acid) diammonium salt (ABTS) were purchased from Sigma-Aldrich Chemical Co. (St. Louis, MO, USA). Glucose oxidase, glucose, fructose, maltose and lactose were obtained from Sangon Biological Engineering Technology & Services Co., Ltd.(Shanghai, China). $H_2O_2$ (30%), $NaCH_2COOH$ (NaAc), and $CH_3COOH$ (HAc) were purchased from Guangfu Chemical Reagent Factory (Tianjin, China). All other chemicals were of analytical grade and used without further purification. Water was purified with a Milli-Q plus 185 equip from Millipore (Bedford, MA, USA) and used throughout all experiments. UV–visible absorption spectra and kinetic measurements were carried out on a Lamda 35 UV-vis spectrophotometer (Perkin-Elmer, USA). Transmission electron microscopy (TEM) images, high-resolution transmission electron microscopy (HRTEM) images and selected are a electron diffraction (SAED) images were performed on a Tecnai G2 TF20 transmission electron microscope (FEI, USA). Scanning electron microscopy (SEM) images were recorded on a JSM−6701F field emission scanning electron microscope (Japan). X-ray diffraction (XRD) patterns were carried out in an X'Pert PRO X-ray diffractometer (PANnalytical, Netherlands). X-ray photoelectron spectra (XPS) analyses were conducted using an

ESCALAB 250Xi X-ray photoelectron spectroscopy (ThermoFisher Scientific, USA).

### 2.2. Preparation of hemin-functionalized $WS_2$ nanosheets

Hemin-functionalized $WS_2$ nanosheets (hemin/$WS_2$-NSs) were prepared based on a previously reported method with minor modifications.[35] Briefly, 50 mL of 26 μg/mL hemin was added to 50 mL of the homogeneous $WS_2$ nanosheets (26 μg/mL) solution, followed by incubating for 4 h at 60 °C. After incubation, the resulting solution was then centrifuged at 16000 rpm for 30 min and black sediments, hemin/$WS_2$-NSs, were obtained. Furthermore, the as-prepared hemin/$WS_2$-NSs were washed by repeated centrifugation (16000 rpm, 30 min) and resuspension in ethanol for three times. And then, the sediments were resuspended in water to prepare the hemin/$WS_2$-NSs solution under sonication.

### 2.3. Detection of $H_2O_2$ and glucose

$H_2O_2$ detection was performed as follows: hemin/$WS_2$-NSs (100 μL, 32 μg/mL), TMB (100 μL, 10 mM) and 600 μL HAc-NaAc buffer (0.2 mM, pH 4.0) were added into a 1.5 mLeppendorf tube. 200 μL of $H_2O_2$ with different concentration was added. Subsequently, the mixed solutions were incubated for 30 min at 40 °C. Finally, 20 μL $H_2SO_4$ (20%, v/v) was added into the above reaction mixture to stop the catalytic reaction, and the absorbance of the resultant mixture at 450 nm was used for quantification of $H_2O_2$. All experiments were repeated three times and each sample solution was measured five times.

Glucose detection was realized as follows: A 20 μL volume of 10 mg/mL GOx solution was added into a 1.5 mL eppendorf tube, followed by the addition of 280 μL HAc-NaAc buffer (0.2 mM, pH 4.0) containing different concentrations of glucose, the resulting solution was maintained at 37 °C for 30 min to produce $H_2O_2$. And then, 100 μL hemin/$WS_2$-NSs (32 μg/mL), 100 μL TMB (10 mM) and 500 μL HAc-NaAc buffer (0.2 mM, pH 4.0) were successively injected into the resulting solution, and allowed to further incubate for 30 min at 40 °C. Finally, 20 μL $H_2SO_4$ (20%, v/v) was added into the above reaction mixture to stop the catalytic reaction, and the absorbance of the resultant mixture at 450 nm was used for quantification of glucose. All experiments were repeated three times and each sample solution was measured five times.

## 3. Results and discussion

### 3.1. Characterization of $WS_2$ nanosheets

Fig. S1(A) showed a TEM image of layered $WS_2$ nanosheets. The SAED pattern of $WS_2$ nanosheets as an inset image in Fig. S1(B) reveals a crystal structure and diffraction points of (101) and (110) planes. The HRTEM image (Fig. S1(C), (D)) clearly illustrated the periodic atomic arrangement of the $WS_2$ nanosheets with a layer separation of about 2.64 Å assigned to the $WS_2$ (101) plane.

### 3.2. Formation of hemin-functionalized $WS_2$ nanosheets

UV-vis absorption spectra were used to characterize the formation of hemin-functionalized $WS_2$ nanosheets. As shown in Fig. 1, the $WS_2$-NSs dispersion displays a characteristic peak at around 241 nm and 625 nm, which was consistent with previous reports (Fig. 1 curve a).[36,37] The spectrum of hemin solution shows a strong peak at around 400 nm attributed to the Soret band, as well as a group of weak peaks between 500 and 700 nm ascribed to the Q-bands (Fig. 1

curve c). After reduction, the color of the WS$_2$-NSs dispersion changes from pale-yellow (Fig. 1, inset a) to brown (Fig. 1, inset b). The hemin/WS$_2$-NSs aqueous dispersion exhibit a broad absorption at 254 nm, which corresponds to the characteristic peaks of WS$_2$-NSs with a large bathochromic shift and a broad absorption peak was observed at around 400 nm, close to the Soret band of hemin. It is clearly demonstrated that WS$_2$-NSs adsorbed hemin molecules at the surface of nanosheets through van der Waals interactions, which allowed them to be well dispersed in ethanol solution, where a characteristic absorption of hemin was observed from complex nanosheets. Particularly, the dispersion is stable and no obvious precipitates are observed after being stored for more than 3 months.
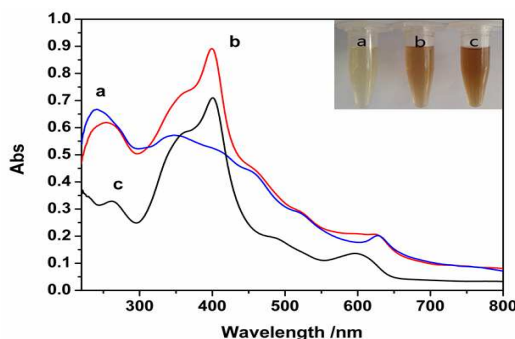


**Fig. 1** UV-visible spectra of WS$_2$-NSs suspension (a), hemin/WS$_2$-NSs suspension (b), hemin solution (c). Inset: photographs of WS$_2$-NSs (a), hemin/WS$_2$-NSs (b), hemin solution (c).

The SEM images of the as-prepared WS$_2$-NSs and hemin/WS$_2$-NSs are shown in Fig. S2(A) and (B), respectively, which were used to confirm the nanosheet structure of hemin/WS$_2$-NSs, indicating that hemin molecules adsorbed on the surface of WS$_2$-NSs would not break their original nanosheet morphology. To confirm the chemical composition, the XPS survey of WS$_2$-NSs and as-prepared hemin/WS$_2$-NSs were clearly illustrated in Fig. 2 (A). As seen in this figure, the relative intensities of C 1s and O 1s binding energy at hemin/WS$_2$-NSs increase significantly when compared to that of WS$_2$-NSs. Meanwhile, a weak peak related to Fe 2p binding energy appears, indicating the formation of hemin/WS$_2$-NSs. X-ray diffraction (XRD) spectra was employed to further explore the crystal structures of WS$_2$-NSs and hemin/WS$_2$-NSs. The results obtained are presented in Fig. 2(B). It can be seen that both WS$_2$-NSs and hemin/WS$_2$-NSs are mainly identifed as 2H WS$_2$, which have a dominant peak appearing at 14.36°, representing the (002) plane (PDF card no. 8724-17).
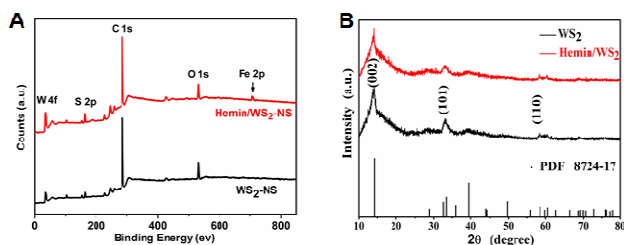


**Fig. 2** (A) XPS survey of WS$_2$-NSs and hemin/WS$_2$-NSs. (B) XRD patterns of WS$_2$-NSs and as-prepared hemin/WS$_2$-NSs.

## 3.2. Peroxidase-like activity of hemin/WS$_2$-NSs

It is well known that peroxidase can catalyze the oxidation of a peroxidase substrate to produce a color change. To assess the peroxidase-like activity of the hemin/WS$_2$-NSs, TMB–H$_2$O$_2$ reaction was used as a model reaction system. The peroxidase-like activity of hemin/WS$_2$-NSs was first evaluated by the catalytic oxidation of peroxidase substrate TMB in the presence of H$_2$O$_2$ to produce the typical blue color reaction (Fig. S3) with maximum absorbance at 369 nm and 652 nm, increased with the increasing of reaction time (Fig. 3A), which originates from the one-electron oxidation of TMB. However, only addition of H$_2$O$_2$ or hemin/WS$_2$-NSs to TMB solution the absorbance at 652 nm displayed negligible change (Fig. 3B), indicating no oxidation reaction occurred. These results clearly indicated hemin/WS$_2$-NSs exhibited intrinsic peroxidase-like activity and not only H$_2$O$_2$ but hemin/WS$_2$-NSs were required for the reaction, as was also the case for horseradish peroxidase (HRP). Hemin is the activate site in peroxidase enzyme, and exhibits the catalytic activity similar to the peroxidase enzyme. It is also reported that WS$_2$-NSs possess intrinsic peroxidase-like activity. As shown Fig. 4. For a comparison study, the response of TMB–H$_2$O$_2$ system was also investigated in the presence of hemin alone or WS$_2$-NSs alone. The results showed that the hemin/WS$_2$-NSs exhibited much higher activity than hemin itself or WS$_2$-NSs alone. To further investigate the catalytic activity of hemin/WS$_2$-NSs, we compared the catalytic activity with hemin and WS$_2$-NSs at the different concentrations of H$_2$O$_2$ (Fig. S4). We could see that the hemin/WS$_2$-NSs exhibited much higher activity than hemin itself or WS$_2$-NSs alone. So, the synergetic effects between hemin and WS$_2$-NSs would result in the high catalytic activity of hemin/WS$_2$-NSs. The peroxidase-like activity of hemin/WS$_2$-NSs was further confirmed by the catalytic oxidation of other peroxidase substrates such as ABTS and OPD in the presence of H$_2$O$_2$. The results are shown in Fig. S5. It can be seen from Fig. S5 that hemin/WS$_2$-NSs could catalyze ABTS to give a green color and catalyze OPD to give an orange color.
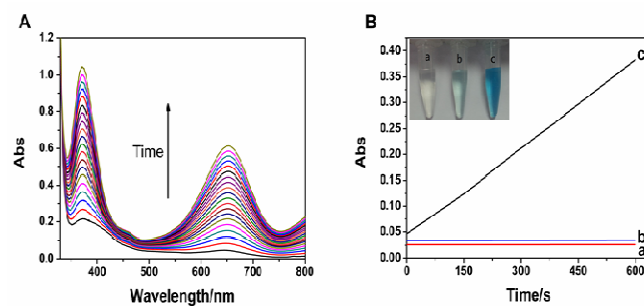


**Fig. 3** (A) The UV-visible absorption spectra change in the system of hemin/WS$_2$-NSs + TMB + H$_2$O$_2$ with the reaction time. The concentration of hemin/WS$_2$-NSs, TMB, and H$_2$O$_2$ are 3.2 μg mL$^{-1}$, 1.0 mmol L$^{-1}$, 0.08 mmol L$^{-1}$, respectively.(B) Time-dependent absorbance changes at 652 nm of TMB solution in different reaction systems. (a) TMB + H$_2$O$_2$, (b) hemin/WS$_2$-NSs + TMB, and (c) hemin/WS$_2$-NSs + TMB + H$_2$O$_2$. Inset shows the photos of the reaction system (a), (b), and (c), respectively.

In order to further improve the peroxidase-like activity of hemin/WS$_2$-NSs, substrates TMB and H$_2$O$_2$ was used as a proof-of-principle reaction system. As expected, like HRP and NPs-based peroxidase mimetics, the catalytic activity of hemin/WS$_2$-NSs is also dependent on temperature, pH, and H$_2$O$_2$ concentration. The catalytic activity was increased with the increasing of catalyst concentration and reaction time. The catalytic activity was increased with the reaction time and slowed down after 30 min. It was reported that the catalytic activity of HRP was largely inhibited after

incubation at pH lower than 4.0 or temperature higher than 50 °C.[13] In contrast, hemin/WS₂-NSs exhibited high catalytic activity over a wide range of pH (2.0–7.0) and temperature (30–60 °C), the robustness of hemin/WS₂-NSs make them potentially applicable under harsh conditions (Fig. S6). Like HRP and other nanomaterials-based peroxidase mimics, the catalytic activity of hemin/WS₂-NSs was inhibited at high $H_2O_2$ concentration. Under our experimental conditions, the optimal temperature, reaction time, $H_2O_2$ concentration, and pH are 40 °C, 30 min,150 mmol L$^{-1}$, and 4.0, respectively.
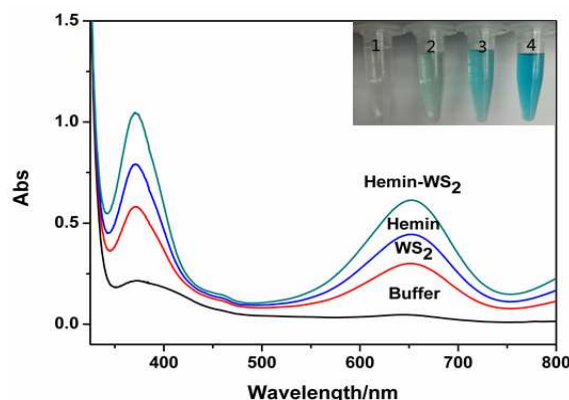


**Fig. 4** Absorption spectra of TMB–$H_2O_2$ mixed solution in the absence of catalyst (black line), and in the presence of 3.2 μg mL$^{-1}$ WS₂-NSs (red line), 3.2 μg mL$^{-1}$ hemin (blue line) and 3.2 μg mL$^{-1}$ hemin/WS₂-NSs (green line), respectively. The insert shows the corresponding optical photographs of the TMB–$H_2O_2$ mixed solution in the absence of catalyst (1), and in the presence of hemin (2), WS₂-NSs (3), and hemin/WS₂-NSs (4).

## 3.3. Kinetic analysis

To investigate the catalytic mechanism of the peroxidase-like activity of the hemin/WS₂-NSs, apparent steady-state kinetic parameters for the peroxidase-like color changing reaction were determined by changing the concentrations of TMB or $H_2O_2$ in this system while keeping the other one constant. Kinetic experiments were carried out using 100 μL of hemin/WS₂-NSs in 1.0 mL of NaAc–HAc buffer solution (0.2 mM, pH 4) containing 1.0 mM TMB as the substrate, and the $H_2O_2$ concentration was 0.12 mM. The initial reaction rate was calculated using the Lambert-Beer Law

$$c = \frac{A}{\varepsilon b}$$ where, b is the thickness of the solution, A is the absorbance,

c is the substrate concentration. The absorbance data were back-calculated to give concentrations using a molar absorption coefficient, ε, of 39 000 M$^{-1}$cm$^{-1}$ for the TMB derived oxidation products.[18] The Michaelis–Menten constant (Km) and maximum initial velocity (Vmax) were obtained from Lineweaver–Burk plots of the double reciprocal of the Michaelis–Menten equation, 1/ν = (Km/Vmax)×(1/[S])＋1/Vmax, where ν is the initial velocity, Vmax is the maximal reaction velocity, Km is the Michaelis–Menten constant and [S] is the concentration of the substrate. All results are shown in Fig.5, The results demonstrated that the oxidation reaction catalyzed by hemin/WS₂-NSs agreed with the typical Michaelis–Menten behavior towards both substrates TMB and $H_2O_2$. The double-reciprocal plots (Fig.5 C and D) revealed the characteristic parallel lines of a ping-pong mechanism and implied that

hemin/WS₂-NSs bound and reacted with the first substrate (TMB or $H_2O_2$), then released the first product before reacting with the second substrate ($H_2O_2$ or TMB). The Michaelis constant (Km) and reaction rate (Vmax) were obtained from Line weaver–Burk plots (Table S1). From Table S1, the apparent Km value of hemin/WS₂-NSs with $H_2O_2$ as the substrate was significantly lower than HRP, indicating that hemin/WS₂-NSs has higher catalytic activity to $H_2O_2$ than HRP. The apparent Km value of hemin/WS₂-NSs with TMB as the substrate was higher than HRP, consistent with the observation that a higher TMB concentration was needed to obtain the max activity of hemin-functionalized WS₂ nanosheets. By comparing the apparent kinetic parameters, the Km value of hemin/WS₂-NSs with $H_2O_2$ as the substrate was  lower than that of hemin and higher than that of WS₂-NSs. The interaction between hemin and WS₂-NSs leads to the catalytic activity of hemin/WS₂-NSs. The catalytic activity of hemin/WS₂ is mainly attributed to both of them.
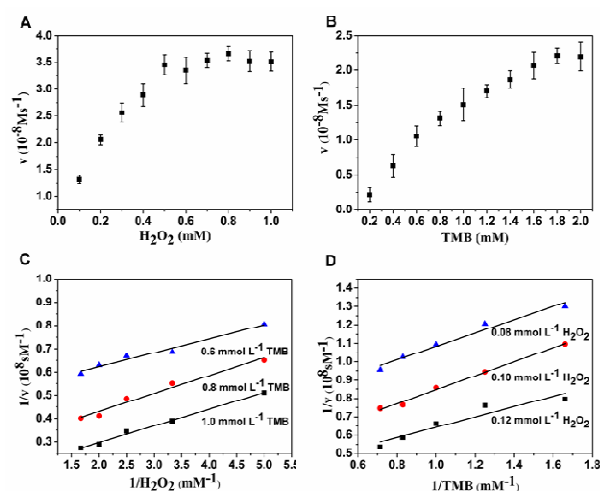


**Fig. 5** Steady-state kinetic assay and catalytic mechanism of hemin/WS₂-NSs (A–D). The velocity (v) of the reaction was measured using hemin/WS₂-NSs (3.2 μg mL$^{-1}$) in HAc-NaAc buffer (0.2 mM, pH 4.0) at 40 °C. The error bars represent the standard error derived from three repeated measurements. (A) The concentration of TMB was 1.0 mmol L$^{-1}$, and the $H_2O_2$ concentration was varied. (B) The concentration of $H_2O_2$ was 0.12 mmol L$^{-1}$, and the TMB concentration was varied. (C, D) Double reciprocal plots of activity of hemin/WS₂-NSs with the concentration of one substrate (TMB or $H_2O_2$) fixed and the other varied.

## 3.4. Detection of $H_2O_2$ and glucose

On the basis of the above optimum assay conditions, we evaluated the sensitivity of the proposed label-free colorimetric method for the detection of $H_2O_2$ and glucose. Fig. 6A depicts a typical $H_2O_2$ concentration-dependent absorbance changes curve at 450 nm upon analyzing different concentrations of $H_2O_2$. As higher concentrations of $H_2O_2$ were added, the absorbance values increased. Fig. 6B exhibits a good linear relationship between the aborsorption intensity and $H_2O_2$ concentration from 5 to 140 μmol (R$^2$=0.9944). The limit of detection was estimated to be 1.0 μmol from three times the standard deviation corresponding to the blank sample detection, which was lower than that reported in most of the previous reports (Table S2[a)]). To explore the selectivity of the novel $H_2O_2$ sensing system, the catalytic reaction was further investigated at the presence of some common impurities such as NaCl, KCl, CaCl₂, ascorbic

acid, dopamine, cysteine, ClO⁻ and $Cr_2O_7^{2-}$. When the concentrations of inorganic salts were higher than 0.5 M, hemin/$WS_2$-NSs were observed to aggregate in salt solution because of the charge screening effects.[35] Furthermore, when the concentrations of the small biological molecules were lower than 10 mM, they did not disturb the determination of $H_2O_2$ (Tabel S3). These results clearly demonstrated that our proposed sensor could be used to detect $H_2O_2$ in the presence of other oxidants because of its great selectivity. When combined with glucose oxidase (GOx), GOx catalyzed the oxidation of glucose to gluconic acid in HAc-NaAc buffer solution, and oxygen in solution was converted to $H_2O_2$, which would oxidize TMB to produce a blue-color product via the catalysis of hemin-functionalized $WS_2$ nanosheets. this indicates that proposed label colorimetric method could also be used for the determination of glucose, which is an important indicator for the diagnosis of diabetes in clinical medicine.[17,18] As illustrated in Fig. 7A, the aborsorption intensity of this solution at 450 nm gradually increased with the increasing of glucose concentration. The linear range for glucose (Fig. 7B) was from 5 to 200 μmol L⁻¹ (R²=0.9983) with a limit of detection of 1.5 μmol L⁻¹, which was more sensitive than that reported in most of the previous reports (Table S2[b]).
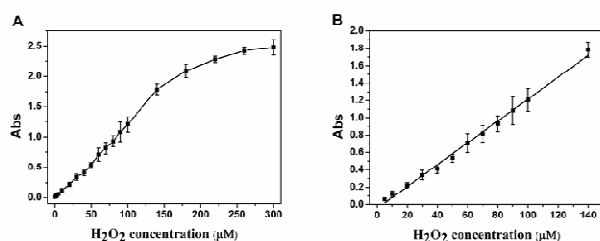


**Fig. 6** (A) A dose–response curve for $H_2O_2$ detection and (B) the linear calibration plot for $H_2O_2$. The error bars represent the standard deviation of three measurements.
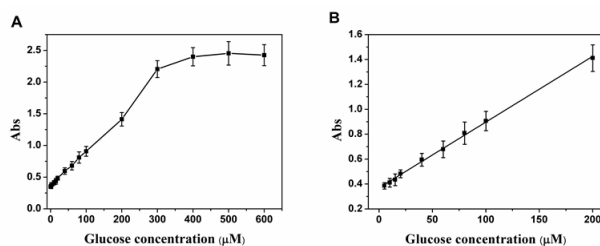


**Fig. 7** (A) A dose–response curve for glucose detection and (B) the linear calibration plot for glucose. The error bars represent the standard deviation of three measurements.

In order to further explore the selectivity of this novel glucose sensing system, a comparison of the aborsorption intensity induced by fructose, lactose and maltose were performed. As illustrated in Fig. S7, the results demonstrated that the absorbance of these glucose analogues was negligible compared with that of glucose even at concentrations as high as 5 mM. This indicates that this sensing system has a high selectivity for glucose detection, which could be attributed to the high affinity of glucose oxidase for glucose. Finally, in order to evaluate the applicability of the proposed method based on the Hemin/$WS_2$-NSs for the determination of glucose in complex biological samples. The present label-free colorimetric

assay was used to quantify glucose in three human serum amples from healthy individuals. The results of the determination and recovery are shown in Table S4. One observed that the recoveries are ranged from 99.0% to 102%, and the relative standard deviations are from 1.6% to 4.0%. These results indicate the validity of the proposed label-free colorimetric method for the determination of glucose in real biological samples.

## 4. Conclusions

In summary, we provide the first report that hemin-functionalized $WS_2$ nanosheets exhibit intrinsic peroxidase-like activity, which follows the typical Michaelis–Menten kinetics and ping-pong mechanism. Meanwhile, as a new support of hemin, $WS_2$ nanosheets were presented, showing their strong van der Waals force when interacting with plane-like molecules. In addition, the hemin/$WS_2$-NSs as peroxidase mimetics show several advantages over HRP and other peroxidase nanomimetics, such as ease of preparation, stability, dispersibility, high catalytic efficiency and low-cost. The hemin/$WS_2$-NSs can be successfully used for label-free, sensitive and highly selective colorimetric detection of $H_2O_2$ and glucose. In consideration of these advantages, we believe that the new prepared hemin/$WS_2$-NSs would have potential applications in environmental chemistry, biotechnology and clinical diagnostic.

## Acknowledgements

## Notes and references

a Key Laboratory of Chemistry of Northwestern Plant Resources, Key Laboratory for Natural Medicine of Gansu Province, Lanzhou Institute of Chemical Physics, Chinese Academy of Sciences, Lanzhou 730000, China. E-mail: hdqiu@licp.cas.cn (H. Qiu); Fax: +86 931 8277088; Tel.: +86 931 4968877.
b School of Materials Science and Engineering, Key Laboratory for Advanced Technologies of Materials of the Ministry of Education, Southwest Jiaotong University, Chengdu 610031, China.

1  K. Saha, S. S. Agasti, C. Kim, X. Li and V. M. Rotello, *Chem. Rev.,* 2012, **112**, 2739–2779.

2  J. Du, L. Jiang, Q. Shao, X. Liu, R. S. Marks, J. Ma and X. Chen, *Small.,* 2013, **9**, 1467–1481.

3  M. E. Stewart, C. R. Anderton, L. B. Thompson, J. Maria, S. K. Gray, J. A. Rogers and R. G. Nuzzo, *Chem. Rev.,* 2008, **108,** 494−521.

4  M. De, P. S. Ghosh and V. M. Rotello, *Adv. Mater.,* 2008, **20**, 4225−4241.

5  J. Liu, Z. Cao and Y. Lu, Chem. Rev., 2009, 109, 1948−1998.

6   S. Song, Y. Qin, Y. He, Q. Huang, C. Fan and H. Y. Chen, *Chem. Soc. Rev*., 2010, **39**, 4234−4243.

7   H. Wei and E. Wang, *Chem. Soc. Rev*., 2013, **42**, 6060–6093.

8   J. Xie, X. Zhang, H. Wang, H. Zheng and Y. Huang, *TrAC, Trends Anal. Chem*., 2012, **39**, 114–129.

9   L. Gao, J. Wu, S. Lyle, K. Zehr, L. Cao and D. Gao, *J. Phys. Chem. C*., 2008, **112**, 17357−17361.

10  L. Z. Gao, J. Zhuang, L. Nie, J. B. Zhang, Y. Zhang, N. Gu, T. H. Wang, J. Feng, D. L. Yang, S. Perrett and X. Yan, *Nat. Nanotechnol*., 2007, **2**, 577−583.

11  T. Lin, L. Zhong, L. Guo, F. Fu and G. Chen, *Nanoscale*, 2014, **6**, 11856–11862.

12  L. Su, J. Feng, X. Zhou, C. Ren, H. Li and X. Chen, *Anal. Chem*., 2012, **84**, 5753−5758.

13  J. Mu, Y. Wang, M. Zhao and L. Zhang, *Chem. Commun*., 2012, **48**, 2540−2542.

14  R. Andre, F. Natalio, M. Humanes, J. Leppin, K. Heinze, R. Wever, H. C. Schroeder, W. E. G. Mueller and W. Tremel, *Adv. Funct. Mater*., 2011, **21**, 501−509.

15  Y. J. Song, X. H. Wang, C. Zhao, K. G. Qu, J. S. Ren and X. G. Qu, *Chem.−Eur. J*., 2010, **16**, 3617−3621.

16  R. J. Cui, Z. D. Han and J. J. Zhu, *Chem.−Eur. J*., 2011, **17**, 9377− 9384.

17  Y. J. Song, K. G. Qu, C. Zhao, J. S. Ren and X. G. Qu, *Adv. Mater*., 2010, **22**, 2206−2210.

18  W. B. Shi, Q. L. Wang, Y. J. Long, Z. L. Cheng, S. H. Chen, H. Z. Zheng and Y. M. Huang, *Chem. Commun*., 2011, **47**, 6695−6697.

19  X. H. Wang, K. G. Qu, B. L. Xu, J. S. Ren and X. G. Qu, *Nano Res*., 2011, **4**, 908−920.

20  H. Wei and E. Wang, *Anal. Chem*., 2008, **80**, 2250−2254.

21  N. Ding, N. Yan, C. Ren and X. Chen, *Anal. Chem*., 2010, **82**, 5897−5899.

22  H. R. Gutiérrez, N. Perea-Lopez, A. L. Elias, A. Berkdemir, B. Wang, R. Lv, F. Lopez-Urias, V. H. Crespi, H. Terrones and M. Terrones, *Nano Lett., 2*013, **13**, 3447–3454.

23  W. Zhao, Z. Ghorannevis, L. Chu, M. Toh, C. Kloc, P.-H. Tan and G. Eda, *Nano Lett*., 2013, **7**, 791–797.

24  D. Voiry, H. Yamaguchi, J. Li, R. Silva, D. C. B. Alves, T. Fujita, M. Chen, T. Asefa, V. B. Shenoy, G. Eda and M. Chhowalla, *Nat. Mater*., 2013, **12**, 850–855.

25  J. Yang, D. Voiry, S. J. Ahn, D. Kang, A. Y. Kim, M. Chhowalla and H. S. Shin, *Angew.Chem., Int.Ed*., 2013, **52**, 13751–13754.

26  H. Liu, D. Su, G. Wang and S. Z. Qiao, *J. Mater.Chem*., 2012, **22**, 17437–17440.

27  T. Georgiou, R. Jalil, B. D. Belle, L. Britnell, R. V. Gorbachev, S. V. Morozov, Y.-J. Kim, A. Gholinia, S. J. Haigh and O. Makarovsky, *Nat. Nanotechnol*., 2012, **8**, 100–103.

28  L. Cheng, J. Liu, X. Gu, H. Gong, X. Shi, T. Liu, C. Wang, X. Wang, G. Liu, H. Xing, W. Bu, B. Sun and Z. Liu, *Adv. Mater*., 2014, **26**, 1886–1893.

29  S. Wang, Y. Zhang, Y. Ning and G.-J. Zhang, *Analyst,* 2015, **140**, 434–439.

30  Q. Xi, D.-M. Zhou, Y.-Y. Kan , J. Ge, Z.-K. Wu, R.-Q. Yu and J.-H. Jiang, *Anal. Chem*., 2014, **86**, 1361–1365.

31  T. Lin, L. Zhong, Z. Song, L. Guo, H. Wu, Q. Guo, Y. Chen, F. Fu and G. Chen, *Biosens.Bioelectron*., 2014, **62**, 302–307.

32  G. Zhang, P. K. Dasgupta, *Anal. Chem*., 1992, **64**, 517–522.

33  Y. Xu, Z. Liu, X. Zhang, Y. Wang, J. Tian, Y. Huang, Y. Ma, X. Zhang and Y. Chen, *Adv. Mater*., 2009, **21**, 1275–1279.

34  J. Geng and H.-T. Jung, *J. Phys. Chem. C*., 2010, **114**, 8227–8234.

35  Y. J. Guo, L. Deng, J. Li, S. J. Guo, E. K. Wang and S. J. Dong, *ACS Nano.,* 2011, **5**, 1282–1290.

36  J. N. Coleman, M. Lotya, A. O'Neill, S. D. Bergin, P. J. King, U. Khan, K. Young, A. Gaucher, S. De, R. J. Smith, I. V. Shvets, S. K. Arora, G. Stanton, H.-Y. Kim, K. Lee, G. T. Kim, G. S. Duesberg, T. Hallam, J. J. Boland, J. J. Wang, J. F. Donegan, J. C. Grunlan, G. Moriarty, A. Shmeliov, R. J. Nicholls, J. M. Perkins, E. M. Grieveson, K. Theuwissen, D. W. McComb, P. D. Nellist and V. Nicolosi, *Science* 2011, **331**, 568–571.

37  K. G. Zhou, N. N. Mao, H. X. Wang, Y. Peng and H. L. Zhang, *Angew. Chem., Int. Ed*., 2011, **50**,10839–10842.

**Analyst Accepted Manuscript**